

# UC Santa Barbara

## UC Santa Barbara Previously Published Works

### Title

PET/CT Imaging of Chemokine Receptors in Inflammatory Atherosclerosis Using Targeted Nanoparticles

### Permalink

<https://escholarship.org/uc/item/6rp005gq>

### Journal

Journal of Nuclear Medicine, 57(7)

### ISSN

0161-5505

### Authors

Luehmann, Hannah P  
Detering, Lisa  
Fors, Brett P  
[et al.](#)

### Publication Date

2016-07-01

### DOI

10.2967/jnumed.115.166751

Peer reviewed



Published in final edited form as:

*J Nucl Med.* 2016 July ; 57(7): 1124–1129. doi:10.2967/jnumed.115.166751.

## PET/CT Imaging of Chemokine Receptors in Inflammatory Atherosclerosis Using Targeted Nanoparticles

Hannah P. Luehmann<sup>1</sup>, Lisa Detering<sup>1</sup>, Brett P. Fors<sup>2</sup>, Eric D. Pressly<sup>2</sup>, Pamela K. Woodard<sup>1</sup>, Gwendalyn J. Randolph<sup>3</sup>, Robert J. Gropler<sup>1</sup>, Craig J. Hawker<sup>2</sup>, and Yongjian Liu<sup>1</sup>

Hannah P. Luehmann: Luehmannh@mir.wustl.edu

<sup>1</sup>Department of Radiology, Washington University, Campus Box 8225, 510 S. Kingshighway Blvd., St. Louis, MO 63110

<sup>2</sup>Department of Materials, Chemistry and Biochemistry, University of California, Santa Barbara, California

<sup>3</sup>Department of Pathology and Immunology, Washington University, St Louis, Missouri

### Abstract

Atherosclerosis is inherently an inflammatory process that is strongly affected by the chemokine/chemokine receptors axes regulating the trafficking of inflammatory cells at all stages of the disease. Of the chemokine receptor family, some specifically up-regulated on macrophages play a critical role in plaque development and may have the potential to track plaque progression. However, the diagnostic potential of these chemokine receptors has not been fully realized. Based on our previous work using a broad-spectrum peptide antagonist imaging 8 chemokine receptors together, the purpose of this study was to develop a targeted nanoparticle for sensitive and specific detection of these chemokine receptors in both a mouse vascular injury model and a spontaneously developed mouse atherosclerosis model.

**Methods**—The viral macrophage inflammatory protein-II (vMIP-II) was conjugated to a biocompatible poly(methyl methacrylate)-core/polyethylene glycol-shell amphiphilic comb-like nanoparticle through controlled conjugation and polymerization before radiolabeling with <sup>64</sup>Cu for PET imaging in an apolipoprotein E-deficient (ApoE<sup>-/-</sup>) mouse vascular injury model and a spontaneous ApoE<sup>-/-</sup> mouse atherosclerosis model. Histology, immunohistochemistry, and real-time reverse transcription polymerase chain reaction (RT-PCR) were performed to assess the plaque progression and up-regulation of chemokine receptors.

**Results**—The chemokine receptors targeted <sup>64</sup>Cu-vMIP-II-Comb showed extended blood retention and improved biodistribution. PET imaging showed specific tracer accumulation at plaques in ApoE<sup>-/-</sup> mice, confirmed by competitive receptor blocking studies and assessment in wild-type mice. Histopathological characterization showed the progression of plaque including size and macrophage population, corresponding to the elevated concentration of chemokine receptors and more importantly increased PET signals.

**Conclusion**—This work provides a useful nanoplatform for sensitive and specific detection of chemokine receptors to assess plaque progression in mouse atherosclerosis models.

### Keywords

PET/CT; viral macrophage inflammatory protein-II; chemokine receptor; nanoparticle; atherosclerosis

Atherosclerosis is essentially an inflammatory disease, where inflammation has critical roles in the initiation, progression, and eventual clinical event. Of many studies identifying biomarkers in atherosclerosis, most have centered on addressing leukocyte influx in plaque initiation. This establishes a prime role for selectin family members (i.e. E-selectin) in the capture, tethering, and rolling of circulating monocytes onto the inflamed endothelium and for endothelial adhesion molecules (e.g. ICAM-1, VCAM-1) that mediate leukocyte arrest by interacting with integrins on activated monocytes (1-3). However, leukocyte influx in advanced plaque has shown large variability during the progression of atherosclerosis, which significantly affects the expression of associated biomarkers and requires further studies to investigate the correlation of their expression with the maturation of disease (4-6).

Chemokines are a group of small heparin-binding proteins significantly involved in plaque initiation, progression, destabilization, and rupture due to their critical roles in directing the movement of circulating leukocytes to sites of inflammation or injury through corresponding chemokine receptors (4,7,8). During this longitudinal process, the altered plaque composition is translated in a changed panel of secretory mediators and chemokine receptors (9-13). Due to the promiscuous binding nature of chemokines to their receptors, there are approximately 10 chemokine receptors identified at the atherosclerotic lesions including CCR1, CCR2, CCR3, CCR4, CCR5, CCR8, CXCR2, CXCR3, CXCR4, and CX3CR1. These receptors are actively expressed in inflammatory cells such as macrophages/monocytes and play fundamental roles from the initiation to progression of atherosclerotic plaque (14-17). Preclinical studies showed that the progression of atherosclerotic lesions correlates well with an increase of chemokine receptor concentration expressed within aortas, which not only makes chemokine receptors interesting targets to monitor atherosclerosis progression (18,19), but also therapeutic biomarkers for specific intervention through nanoplatforms (20,21). However, the targeting efficiency and specificity of these nanoprobables needs significant improvement.

Previously, we have developed a vMIP-II peptide based PET tracer ( $^{64}\text{Cu}$ -DOTA-vMIP-II) specifically imaging the up-regulation of a group of chemokine receptors expressed at the injured femoral artery of ApoE<sup>-/-</sup> mice (22). However, the detection sensitivity and specificity need further improvement due to the fast renal clearance of the tracer. Herein, we prepared a comb-like nanoparticle conjugated with multiple copies of vMIP-II peptide and radiolabeled with  $^{64}\text{Cu}$  ( $^{64}\text{Cu}$ -vMIP-II-Comb) to enhance the systemic circulation and improve the detection sensitivity and specificity in the ApoE<sup>-/-</sup> mouse vascular injury model (23-25). Furthermore, this  $^{64}\text{Cu}$ -vMIP-II-Comb was used to measure the spatial and temporal expression patterns of these receptors up-regulated at the aortic arch of ApoE<sup>-/-</sup> mice along the progression of plaque with PET/CT. The quantitative tracer uptake was

correlated to the RT-PCR measurement of chemokine receptors expression, histology, macrophage population and plaque size.

## MATERIALS AND METHODS

Materials were purchased from Sigma-Aldrich and used without further purification unless otherwise stated. The  $^{64}\text{Cu}$  (half-life = 12.7 h,  $\beta^+$  = 17%,  $\beta^-$  = 40%) was produced at the Washington University (26). Functionalized poly(ethylene glycol) (PEG) derivatives were obtained from Intezyne Technologies. Tris-t-butylester-DOTA, 1,4,7,10-tetraazacyclododecane, and DOTA-N-hydroxysuccinimide ester were purchased from Macrocyclics. Viral macrophage inflammatory protein-II (vMIP-II) was customized by CPC scientific. DOTA methacrylate, dithioester Radical Addition Fragmentation Transfer (RAFT) agent, control Comb and 4-pentynoic n-hydroxy succinimide ester were also prepared (26-28). Centricon tubes were from Millipore. Zeba desalting spin columns were obtained from Pierce. Reverse phase-high performance liquid chromatography system was equipped with a UV/VIS detector (Dionex), a radioactivity detector (B-FC-3200; BioScan Inc.) and a C-18 analytic column (5 mm,  $4.6 \times 220$  mm; Perkin Elmer). Polymeric materials were characterized by  $^1\text{H}$  and  $^{13}\text{C}$  nuclear magnetic resonance (NMR) spectroscopy using either a Varian 500 MHz or Varian 600 MHz instrument with the residual solvent signal as an internal reference. Gel permeation chromatography was performed in N,N-dimethylformamide on a Waters system equipped with four 5- $\mu\text{m}$  Waters columns ( $300 \times 7.7$  mm) connected in series with increasing pore size ( $10^2$ ,  $10^3$ ,  $10^4$ , and  $10^6$  Å) and Waters 410 differential refractometer index and 996 photodiode array detectors. The molecular weights of the polymers were calculated relative to linear polystyrene or poly(ethylene oxide) standards. Infrared spectra were recorded on a Perkin Elmer Spectrum 100 with a Universal ATR sampling accessory.

### Polymer Synthesis, Deprotection, Assembly and vMIP-II Conjugation

The synthesis of poly(ethylene glycol)  $\alpha$ -bromide methacrylate ( $\alpha$ -Br-PEGMA) and DOTA- $\alpha$ -bromide-Comb was following a previous report and detailed in supporting information. The polymer (15 mg) was deprotected and assembled into particles (Fig. 1) (26). To a 0.5 mL solution of the deprotected and assembled nanoparticles (1 wt %), 250  $\mu\text{L}$  of a 0.4 wt % solution of vMIP-II in an  $\text{NH}_4\text{OAc}$  buffer was added and reacted overnight. The solution was then diluted with water, transferred to centrifugal filtration tube with 50 kDa molecular weight cutoff, and extensively washed with water. The final solution was concentrated to 1 wt% nanoparticles in water using centrifugal filtration. The averaged hydrodynamic size of the vMIP-II-Comb characterized by dynamic light scattering (DLS) was  $15.8 \pm 2.0$  nm with neutral surface charge (zeta potential:  $5.4 \pm 1.1$  mV, Fig. S1). There were approximately 4 vMIP-II peptide and 70 DOTA per nanoparticle. The non-targeted Comb (zeta potential:  $-32 \pm 3$  mV,  $25 \pm 2$  nm) was also prepared (26).

### ApoE<sup>-/-</sup> Mouse Vascular Injury and Spontaneous Atherosclerosis Models

All animal studies were performed in compliance with guidelines set forth by the National Institutes of Health Office of Laboratory Animal Welfare and approved by the Washington University Animal Studies Committee. The mouse vascular injury model was induced in

male apolipoprotein E knock-out (ApoE<sup>-/-</sup>) mice (n=16, 6 weeks old, Taconic Inc.) through wire injury on the right femoral artery (22,23,29,30). The left femoral artery was surgically prepared by undergoing incision and closure without guide wire endothelial injury to serve as the “sham site”. Wild-type (WT) male C57BL/6 mice (n=5) on normal chow underwent the injury procedure were used as control animals. For the spontaneous atherosclerosis mouse model, male ApoE<sup>-/-</sup> 6 wk old mice were fed a high cholesterol diet (HCD) (Harlan Teklad, 42% fat) for 37 wks. Age-matched WT male C57BL/6 mice on normal chow were used as controls. Each mouse was anesthetized with a standard inhaled-anesthetic protocol (1.5%–2% isoflurane) by induction in a chamber, and maintenance anesthesia was administered via a nose cone.

### Biodistribution Studies

The specific activities of <sup>64</sup>Cu-vMIP-II-Comb and <sup>64</sup>Cu-Comb were 3.2 MBq/nmol and 3.7 MBq/nmol, respectively (25). Male WT C57BL/6 mice weighing 20-25 g (n = 4/group) were anesthetized with inhaled isoflurane and approximately 370 KBq of <sup>64</sup>Cu-vMIP-II-Comb (~ 0.12 nmol) in 100 µL of saline were injected via the tail vein. The mice were reanesthetized before they were euthanized by cervical dislocation at each time point (1, 4, 24, and 48 h) after injection. Organs of interest were collected, weighed, and counted in a well γ-counter (Beckman 8000) to calculate the percentage injected dose per gram of tissue (%ID/gram) (31).

### Small Animal PET/CT Imaging

Two and four weeks after the wire injury of the ApoE<sup>-/-</sup> mice, PET/CT was performed to determine the uptake at injured lesions following the injection of 3.7 MBq of <sup>64</sup>Cu-vMIP-II-Comb or <sup>64</sup>Cu-Comb in 100 µL saline *via* the tail vein. PET/CT images were collected at 24 h post injection (p.i.) based on the biodistribution and previous report (23). The ApoE<sup>-/-</sup> mice with spontaneous atherosclerosis lesion and age-matched wild type C57BL/6 mice were scanned at 20 and 37 weeks on HCD with both <sup>64</sup>Cu-vMIP-II-Comb and <sup>64</sup>Cu-Comb (at 24 h p.i.) with Inveon PET/CT (CT: 8 min, 80 kVp, 500 µA, 250ms, 200µm pixel size; PET: 1 frame, 60 min static scan). PET data was analyzed using the manufacturer’s software (ASI Pro or IRW). The tracer uptake at the region of interest (ROI) was calculated as %ID/gram from the maximum a posteriori reconstructed images. After the last scan, the animals were euthanized by cervical dislocation and the femoral vessels and aortic arches were either perfusion-fixed *in situ* with freshly prepared 4% paraformaldehyde in 1× PBS for histopathology and immunohistochemistry or fast frozen for RT-PCR analysis. Competitive receptor blocking studies were performed in both models for <sup>64</sup>Cu-vMIP-II-Comb by co-injection of unlabeled vMIP-II-Comb in 100 fold excess (n=6) followed by PET scans at 24 h p.i.

### Histologic Characterization of Atherosclerotic Plaques and RT-PCR Assay of Chemokine Receptors

Serial sections of mouse aortic arch of 5 µm in thickness were cut from paraformaldehyde-fixed (24 h), paraffin-embedded specimens for hematoxylin and eosin and macrophage (F4/80 mAb, AbD Serotec MCA497BB) staining. Quantification of plaque area and macrophage was calculated with ImageJ software following a published protocol (12).

Tissue RNA was isolated using TRIzol (Invitrogen) per the manufacturer's instruction. RNA isolated from injured and sham femoral arteries was used for real time RT-PCR. Reverse transcription reactions used 1 µg of total RNA, random hexamer priming, and Superscript II reverse transcriptase (Invitrogen). Expression of chemokine receptors and GAPDH were determined using Taqman assays (Invitrogen) and an EcoTM Real-Time PCR System (Illumina) in duplicate in 48-well plates. PCR cycling conditions were as follows: 50°C for 2 min, 95°C for 21 sec and 60°C for 20 sec. GAPDH expression was used as a comparator using Ct calculations.

### Statistical Analysis

Group variation is described as mean ± SD and compared using 1-way ANOVA with a Bonferroni correction. Individual group differences were determined by a 2-tailed Mann-Whitney test. The significance level in all tests was  $p < 0.05$ .

## RESULTS

### Biodistribution of $^{64}\text{Cu}$ -vMIP-II-Comb

Biodistribution of  $^{64}\text{Cu}$ -Comb was previously reported showing moderate blood retention but high mononuclear phagocyte system (MPS) (liver and spleen) accumulation (25) while the  $^{64}\text{Cu}$ -DOTA-vMIP-II peptide tracer alone showed rapid renal clearance (22). At 1 h p.i., the blood retention of  $^{64}\text{Cu}$ -vMIP-II-Comb ( $42.7 \pm 5.9$  %ID/gram) was significantly ( $p < 0.001$ ,  $n=4$ ) higher than that of  $^{64}\text{Cu}$ -Comb ( $25.4 \pm 3.0$  %ID/gram) (Fig. 2). The hepatic ( $7.2 \pm 0.8$  %ID/gram) and splenic ( $5.8 \pm 0.9$  %ID/gram) uptake were about 5 times and 3 times less than those of  $^{64}\text{Cu}$ -Comb, respectively. Consistent with previous reports using Comb nanoparticles with neutral surface charge showing retentive blood circulation (23,25), the blood pool (sum of blood, lung, and heart) retention of  $^{64}\text{Cu}$ -vMIP-II-Comb did not significantly decrease until 24 h p.i. while its liver and spleen localizations (~ 10 %ID/gram for both) were still significantly ( $p < 0.001$ ,  $n = 4$ ) lower than that of  $^{64}\text{Cu}$ -Comb. At 48 h p.i., the blood retention of  $^{64}\text{Cu}$ -vMIP-II-Comb decreased to  $5.1 \pm 0.3$  %ID/gram and the liver and spleen both gradually increased to ~16 %ID/gram. During the 48 h study, the renal and gastrointestinal tract showed constant clearance despite the variations in blood pool and MPS organs.

### PET/CT Imaging

In the vascular injury model, PET/CT imaging with  $^{64}\text{Cu}$ -vMIP-II-Comb at 24 h p.i. showed specific accumulation at the injured femoral artery and weak localization at the sham-operated site (Fig. 3A) at 2 weeks post injury. Quantitative uptake analysis showed the uptake at injury site was  $7.52 \pm 1.67$  %ID/gram, significantly ( $p < 0.001$ ,  $n=6$ ) higher than that of sham site ( $2.18 \pm 0.76$  %ID/gram). Consistent with previous report about the stable uptake at the injured site with  $^{64}\text{Cu}$ -DOTA-vMIP-II peptide tracer alone between 2 and 4 weeks post injury (22), the  $^{64}\text{Cu}$ -vMIP-II-Comb also showed stable uptake at the injured artery ( $6.92 \pm 1.06$  %ID/gram at 4 weeks,  $n=6$ ) during this period (Fig. S2). Compared to the data obtained with  $^{64}\text{Cu}$ -DOTA-vMIP-II, the uptake of  $^{64}\text{Cu}$ -vMIP-II-Comb at both time points was doubled ( $p < 0.005$ ,  $n=6$ ). The competitive PET blocking on the same mice at 3 weeks post injury with the co-injection of unlabeled vMIP-II-Comb resulted in substantial

decrease at the injured site ( $3.35 \pm 0.16$  %ID/gram, n=6) to a level similar to those acquired at sham site (Fig. 3B), which was significantly ( $p < 0.001$ ) lower than the data obtained a week before.

Further, the non-specific retention due to the size of the nanostructure at the injured site was also assessed with non-targeted  $^{64}\text{Cu}$ -Comb. As shown in Fig. 3A, little uptake ( $2.99 \pm 0.38$  %ID/gram) was observed at the injured artery and the uptake analysis demonstrated significantly ( $p < 0.001$ , n=6) lower accumulation at the injury lesion in contrast to the data obtained with targeted  $^{64}\text{Cu}$ -vMIP-II-Comb (Fig. 2B), which was also confirmed by the results acquired at the 4 week time point (Fig. S2). In the ApoE<sup>-/-</sup> mice fed on HCD for 20 weeks,  $^{64}\text{Cu}$ -vMIP-II-Comb showed specific localization ( $6.12 \pm 0.88$  %ID/gram, n=6) at the aortic arch at 24 p.i. while the non-targeted  $^{64}\text{Cu}$ -Comb showed significantly ( $p < 0.005$ , n=4) lower uptake at the lesion ( $3.16 \pm 0.89$  %ID/gram). The target-to-background (T/B) ratio of  $^{64}\text{Cu}$ -vMIP-II-Comb accumulation at the aortic arch to left ventricular cavity was determined as  $0.45 \pm 0.08$  (n=6), significantly ( $p < 0.01$ , n=4-6/group) higher than that of  $^{64}\text{Cu}$ -Comb ( $0.23 \pm 0.11$ , n=4/group). With the progression of atherosclerosis, the plaque uptake of  $^{64}\text{Cu}$ -vMIP-II-Comb at 24 h p.i. significantly ( $p < 0.01$ , n=6) increased to  $8.88 \pm 1.75$  %ID/gram at 37 weeks on HCD while  $^{64}\text{Cu}$ -Comb showed little variation ( $3.10 \pm 1.16$  %ID/gram, n=6) (Figs. 4A and 4B). The T/B ratio of  $^{64}\text{Cu}$ -vMIP-II-Comb also increased to  $0.78 \pm 0.19$  (n=6) while the ratio of  $^{64}\text{Cu}$ -Comb remained constant as 20 weeks ( $0.27 \pm 0.11$ ,  $p < 0.005$ , n=4-6/group). At 48 h p.i., the plaque uptake of  $^{64}\text{Cu}$ -vMIP-II-Comb slightly increased to  $10.0 \pm 0.72$  %ID/gram (Fig. 4B), leading to 2-fold increase of T/B ratio ( $2.38 \pm 0.25$ , n=6/group). The plaque uptake of  $^{64}\text{Cu}$ -Comb hardly changed ( $3.43 \pm 0.32$  %ID/gram, n=4) although the T/B ratio ( $0.82 \pm 0.65$ , n=4/group) increased due to its decreased blood retention. In the age-matched WT mice, the retention of  $^{64}\text{Cu}$ -vMIP-II-Comb at the aortic arch ( $2.66 \pm 0.31$  %ID/gram) was also significantly ( $p < 0.001$ , n=4) lower than the accumulation acquired in ApoE<sup>-/-</sup> mice. More importantly, the competitive receptor blocking study significantly ( $p < 0.002$ , n=4) decreased the accumulation of  $^{64}\text{Cu}$ -vMIP-II-Comb to a level ( $4.31 \pm 1.07$  %ID/gram) similar to that obtained with  $^{64}\text{Cu}$ -Comb (Fig. 4B). Additional autoradiography images of the two nanoprobe in the dissected aortic arches of ApoE<sup>-/-</sup> mice also confirmed the specific targeting of  $^{64}\text{Cu}$ -vMIP-II-Comb (Fig. S3). Consistent with previous studies comparing multivalent nanoparticles to monovalent peptide tracers alone (23,25), the uptake of  $^{64}\text{Cu}$ -vMIP-II-Comb at the aortic arch was two times higher than that acquired with  $^{64}\text{Cu}$ -DOTA-vMIP-II ( $2.72 \pm 0.30$  %ID/gram, T/B =  $0.76 \pm 0.07$ , n=4) at 37 weeks on HCD.

### Histology, Immunohistochemistry, and RT-PCR

The hematoxylin and eosin staining of right femoral arteries harvested from ApoE<sup>-/-</sup> mice at 2 weeks post injury demonstrated significant progression of plaque compared to the sham-operated left femoral artery (Fig. S4) (23). In the ApoE<sup>-/-</sup> spontaneous atherosclerosis mouse model, the formation of plaque was clearly observed at the aortic arch at 20 weeks on HCD diet (Fig. 5A). The macrophage staining with F4/80 mAb showed positive cells on the surface of the plaque (Fig. 5B). Consistent with our previous report about the progression of atherosclerosis (12), the plaque at 37 weeks post HCD showed increased lipid accumulation and became less cellular. The imageJ analysis of advanced plaque showed more than



doubled (2.4 fold) size compared to that measured at 20 weeks post HCD. F4/80 staining showed that most cells on the advanced plaque were positive and the signal was throughout the plaque. The quantification of macrophage area demonstrated 3.2 fold increase from 20 week time point, which led to increased macrophage/plaque ratio from 19.5% at 20 weeks to 26.7% at 37 weeks. For the age-matched WT mice, histological analysis of aortic arch showed intact vasculature and F4/80 staining showed little signal (Fig. S5).

The expression of chemokine receptors on atherosclerotic plaque has been demonstrated in our previous studies (22,23). The quantitative RT-PCR analysis of ApoE<sup>-/-</sup> mice at 2 weeks post injury showed much higher expression of CCR1, CCR2, CCR3, CCR4, CCR5, CCR8, CX3CR1, and CXCR4 in the injured femoral artery in comparison to the data obtained from sham-operated site (Fig. 6A). Compared to the WT mice, the elevated expression of 8 chemokine receptors on the plaque was determined in the ApoE<sup>-/-</sup> spontaneous atherosclerosis mice at 20 weeks on HCD (Fig. 6B). In agreement with the increased size of plaque and macrophage positive plaque area, the difference of chemokine receptor expression between the disease and WT mice was further increased at 37 weeks on HCD, especially for CCR2 (7.5 fold), CCR5 (5.4 fold), CX3CR1 (5.3 fold), and CXCR4 (4.3 fold) (Fig. 6C).

## DISCUSSION

We report here the results of PET/CT imaging of chemokine receptors up-regulated in a vascular injury ApoE<sup>-/-</sup> mouse model and a spontaneous atherosclerosis ApoE<sup>-/-</sup> mouse model with <sup>64</sup>Cu-vMIP-II-Comb. The superiority of targeted imaging using multivalent nanoparticles was demonstrated by comparing to the <sup>64</sup>Cu-DOTA-vMIP-II peptide tracer alone and the non-targeted <sup>64</sup>Cu-Comb. PET imaging showed increased uptake of <sup>64</sup>Cu-vMIP-II-Comb along the progression of plaque in the spontaneous atherosclerosis model, which correlated with the enlarged plaque size, increased macrophage population, and elevated chemokine receptor expression.

It is known that chemokine-chemokine receptor interactions play a key role in the pathogenesis of atherosclerosis by regulating leukocyte trafficking and the inflammatory processes to promote the progression of disease, which leads to the development of many chemokine receptor antagonists for clinical studies by targeting specific chemokine receptor (32). However, most of them have limited efficacy due to the redundancy of chemokine signaling pathways and dynamic and stage-specific expression of chemokine receptors, which makes a broad-spectrum chemokine receptor antagonist a rational and potentially more successful strategy by blocking a group of chemokine receptors at one time (33,34). Previously, we have demonstrated the specific binding of the <sup>64</sup>Cu-DOTA-vMIP-II peptide tracer alone to 8 chemokine in the vascular injury model (22). Due to the fast renal clearance, the detection sensitivity and specificity needs improvement to determine the plaque at early stage when the chemokine receptors expression is low. As shown in Fig. 2, with the conjugation on the biocompatible poly(methyl methacrylate)-core/polyethylene glycol-shell amphiphilic nanoparticles, the blood retention of <sup>64</sup>Cu-vMIP-II-Comb was significantly extended, which led to doubled PET intensity at the injured site. Although the hepatic and splenic accumulation gradually increased during the 48 h study, they were



significantly ( $p < 0.001$ ,  $n=6$ ) lower than those obtained with the non-targeted  $^{64}\text{Cu}$ -Comb, reasonably due to the effect of its neutral surface charge as reported previously (25). In addition, there was constant kidney accumulation, indicating renal clearance. The stomach and intestines uptake suggested later fecal excretion of the nanoparticles reasonably coming from liver. Further, the targeting specificity was also demonstrated by the competitive PET blocking study and significantly lower uptake acquired with  $^{64}\text{Cu}$ -Comb. Consistent with PET imaging, the RT-PCR analysis of the injured femoral artery showed elevated expression of all chemokine receptors compared to the sham-operated artery.

In the ApoE<sup>-/-</sup> mouse spontaneous atherosclerosis model, the targeted  $^{64}\text{Cu}$ -vMIP-II-Comb showed significantly higher accumulation at the aortic arch than that acquired with non-targeted  $^{64}\text{Cu}$ -Comb and  $^{64}\text{Cu}$ -DOTA-vMIP-II peptide tracer alone, especially at extended imaging time point of 48 h p.i., demonstrating the advantage of targeted, long circulating nanoparticles for atherosclerosis PET imaging. The competitive blocking study and the *ex vivo* autoradiography images confirmed the chemokine receptors mediated uptake in the plaque, which was also corroborated by the low retention of  $^{64}\text{Cu}$ -vMIP-II-Comb at the aortic arch of WT mice. In contrast to a previous report using non-targeted nanoparticle for plaque PET imaging (35), quantitative uptake analysis of targeted  $^{64}\text{Cu}$ -vMIP-II-Comb showed higher accumulation in the aorta and greater T/B ratio. With the progression of disease, the plaque size at 37 weeks increased 1.4 fold compared to that measured at 20 weeks, which was in agreement with the increased uptake (45.1%) of  $^{64}\text{Cu}$ -vMIP-II-Comb, confirming our hypothesis of using a broad-spectrum chemokine receptor ligand to determine the plaque burden.

At all stages of plaque, macrophages are the central cells involved, though the complexity of the lesions grows in advanced plaque. It is thought that macrophages are major contributors to the inflammatory response through their secretion of pro-inflammatory mediators such as chemokines to arrest leukocytes to the plaque (35,36). At 20 weeks on HCD, immunohistochemical analysis showed the up-regulation of macrophages on the surface of the plaque. The RT-PCR analysis also demonstrated elevated expression of the 8 chemokine receptors in the plaque of ApoE<sup>-/-</sup> mice compared to WT mice. With the progression of plaque, not only did the histopathological analysis show the complication of plaque, including high lipid accumulation and calcification, but also the elevated expression of macrophages in contrast to the data acquired at 20 weeks on HCD, which was also confirmed by the enlarged plaque size and increased plaque area positive for macrophages. More importantly, the RT-PCR analysis of these chemokine receptors showed the amplified difference between the ApoE<sup>-/-</sup> and WT mice during the atherosclerosis progression, which not only correlated with the progression of plaque properties but also was in agreement with the increased uptake of  $^{64}\text{Cu}$ -vMIP-II-Comb at aortic arch. Currently, there are some PET tracers used in clinical research for atherosclerosis imaging such as  $^{18}\text{F}$ -FDG or  $^{68}\text{Ga}$ -DOTATATE (37). Most of them focus on individual process such as glucose metabolism or single target such as somatostatin receptors. Due to the complex and dynamic nature of the disease, these imaging agents are challenged to connect the plaque progression to the PET signal. However, this broad-spectrum chemokine receptor targeting nanoprobe may be valuable in assessing the plaque burden and activity due to the active expression and critical roles of these receptors for atherosclerosis progression and deliver useful information for

both diagnosis and treatment in translational research given the success of a similar nanostructure for human plaque PET imaging (38).

## CONCLUSION

In this study, we developed a broad-spectrum chemokine receptor antagonist vMIP-II conjugated nanoparticle of  $^{64}\text{Cu}$ -vMIP-II-Comb prepared with controlled physicochemical properties. The extended blood retention and improved targeting efficiency of  $^{64}\text{Cu}$ -vMIP-II-Comb afforded sensitive and specific detection of 8 chemokine receptors up-regulated in a vascular injury mouse model and a spontaneously developed atherosclerosis mouse model. The increased accumulation of  $^{64}\text{Cu}$ -vMIP-II-Comb in plaque during the progression of atherosclerosis was confirmed by RT-PCR analysis of chemokine receptors and in agreement with the histopathological characterization of plaque including enlarged size and increased macrophage content, indicating the potential of  $^{64}\text{Cu}$ -vMIP-II-Comb to determine plaque progression.

## Supplementary Material

Refer to Web version on PubMed Central for supplementary material.

## Acknowledgments

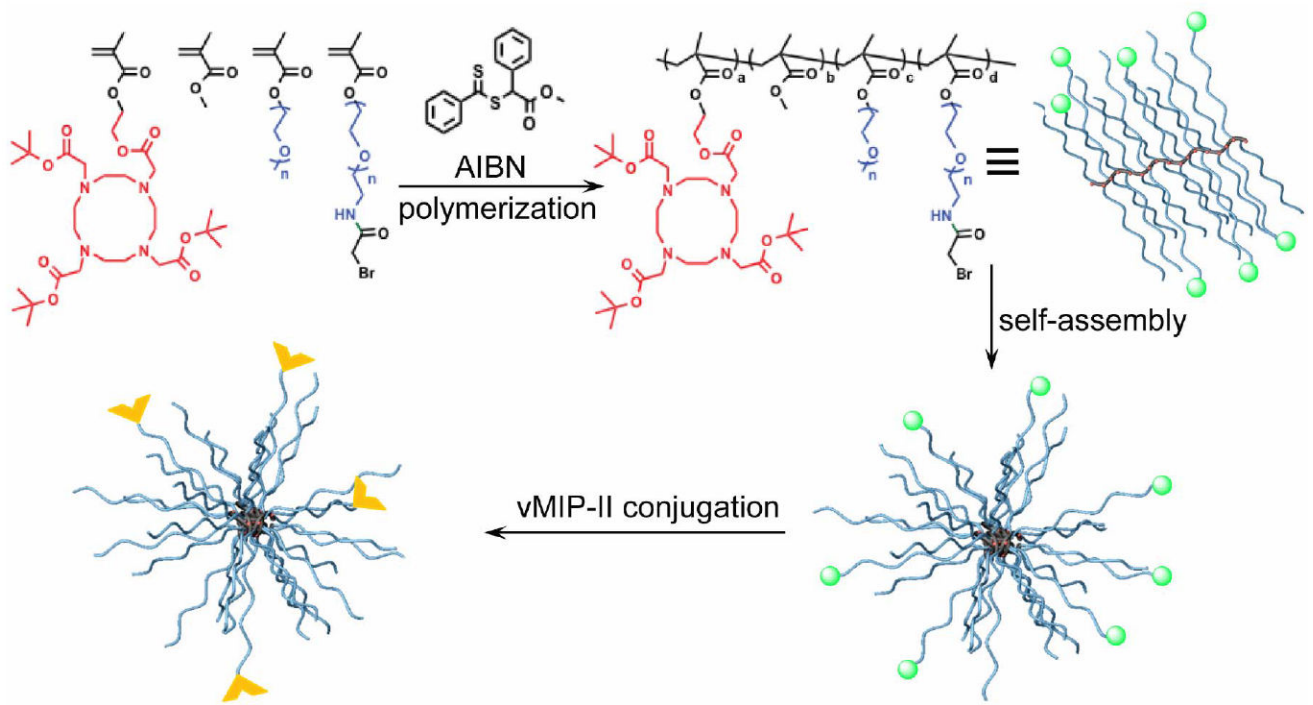
This work is supported by the National Heart, Lung, and Blood Institute as a Program of Excellence in Nanotechnology (HHSN268201000046C) and R01 (1R01HL125655-01).



## References

1. Dong ZM, Brown AA, Wagner DD. Prominent role of P-selectin in the development of advanced atherosclerosis in ApoE-deficient mice. *Circulation*. 2000; 101:2290–2295. [PubMed: 10811597]
2. Nakashima Y, Raines EW, Plump AS, Breslow JL, Ross R. Upregulation of VCAM-1 and ICAM-1 at atherosclerosis-prone sites on the endothelium in the ApoE-deficient mouse. *Arterioscler Thromb Vasc Biol*. 1998; 18:842–851. [PubMed: 9598845]
3. Wildgruber M, Swirski FK, Zerneck A. Molecular Imaging of Inflammation in Atherosclerosis. *Theranostics*. 2013; 3:865–884. [PubMed: 24312156]
4. Kraaijeveld AO, de Jager SC, van Berkel TJ, Biessen EA, Jukema JW. Chemokines and atherosclerotic plaque progression: towards therapeutic targeting? *Curr Pharm Des*. 2007; 13:1039–1052. [PubMed: 17430167]
5. Charo IF, Ransohoff RM. The many roles of chemokines and chemokine receptors in inflammation. *N Engl J Med*. 2006; 354:610–621. [PubMed: 16467548]
6. Libby P. Inflammation in atherosclerosis. *Arterioscler Thromb Vasc Biol*. 2012; 32:2045–2051. [PubMed: 22895665]
7. Braunersreuther V, Mach F, Steffens S. The specific role of chemokines in atherosclerosis. *Thromb Haemost*. 2007; 97:714–721. [PubMed: 17479181]
8. John, AE.; Channon, KM.; Greaves, DR. Chemokines, chemokine receptors and atherosclerosis. In: Schwiebert, LM., editor. *Chemokines, Chemokine Receptors, and Disease*. Amsterdam, The Netherlands: Elsevier; 2005. p. 223-253.
9. Veillard NR, Steffens S, Burger F, Pelli G, Mach F. Differential expression patterns of proinflammatory and antiinflammatory mediators during atherogenesis in mice. *Arterioscler Thromb Vasc Biol*. 2004; 24:2339–2344. [PubMed: 15458979]

10. Veillard NR, Braunersreuther V, Arnaud C, et al. Simvastatin modulates chemokine and chemokine receptor expression by geranylgeranyl isoprenoid pathway in human endothelial cells and macrophages. *Atherosclerosis*. 2006; 188:51–58. [PubMed: 16321392]
11. Gautier EL, Ivanov S, Lesnik P, Randolph GJ. Local apoptosis mediates clearance of macrophages from resolving inflammation in mice. *Blood*. 2013; 122:2714–2722. [PubMed: 23974197]
12. Potteaux S, Gautier EL, Hutchison SB, et al. Suppressed monocyte recruitment drives macrophage removal from atherosclerotic plaques of Apoe<sup>-/-</sup> mice during disease regression. *J Clin Invest*. 2011; 121:2025–2036. [PubMed: 21505265]
13. Tacke F, Alvarez D, Kaplan TJ, et al. Monocyte subsets differentially employ CCR2, CCR5, and CX3CR1 to accumulate within atherosclerotic plaques. *J Clin Invest*. 2007; 117:185–194. [PubMed: 17200718]
14. Quinones MP, Martinez HG, Jimenez F, et al. CC chemokine receptor 5 influences late-stage atherosclerosis. *Atherosclerosis*. 2007; 195:e92–e103. [PubMed: 17466311]
15. Bursill CA, Channon KM, Greaves DR. The role of chemokines in atherosclerosis: recent evidence from experimental models and population genetics. *Curr Opin Lipidol*. 2004; 15:145–149. [PubMed: 15017357]
16. White GE, Iqbal AJ, Greaves DR. CC chemokine receptors and chronic inflammation—therapeutic opportunities and pharmacological challenges. *Pharmacol Rev*. 2013; 65:47–89. [PubMed: 23300131]
17. Zernecke A, Shagdarsuren E, Weber C. Chemokines in atherosclerosis: an update. *Arterioscler Thromb Vasc Biol*. 2008; 28:1897–1908. [PubMed: 18566299]
18. Zernecke A, Weber C. Chemokines in the vascular inflammatory response of atherosclerosis. *Cardiovasc Res*. 2010; 86:192–201. [PubMed: 20007309]
19. Jerath, MR.; Kwan, M.; Liu, P.; Patel, DD. Chemokine receptors in atherosclerosis. In: Harrison, JK.; Lukacs, NW., editors. *The Chemokine Receptors*. Totowa, New Jersey: Humana Press; 2007. p. 199-233.
20. Bahal R, McNeer NA, Ly DH, Saltzman WM, Glazer PM. Nanoparticle for delivery of antisense gammaPNA oligomers targeting CCR5. *Artif DNA PNA XNA*. 2013; 4:49–57. [PubMed: 23954968]
21. Leuschner F, Dutta P, Gorbатов R, et al. Therapeutic siRNA silencing in inflammatory monocytes in mice. *Nat Biotechnol*. 2011; 29:1005–1010. [PubMed: 21983520]
22. Liu Y, Pierce R, Luehmann HP, Sharp TL, Welch MJ. PET imaging of chemokine receptors in vascular injury-accelerated atherosclerosis. *J Nucl Med*. 2013; 54:1135–1141. [PubMed: 23658218]
23. Luehmann HP, Pressly ED, Detering L, et al. PET/CT imaging of chemokine receptor CCR5 in vascular injury model using targeted nanoparticle. *J Nucl Med*. 2014; 55:629–634. [PubMed: 24591489]
24. Liu Y, Welch MJ. Nanoparticles labeled with positron emitting nuclides: advantages, methods, and applications. *Bioconjug Chem*. 2012; 23:671–682. [PubMed: 22242601]
25. Liu Y, Pressly ED, Abendschein DR, et al. Targeting angiogenesis using a C-type atrial natriuretic factor-conjugated nanoprobe and PET. *J Nucl Med*. 2011; 52:1956–1963. [PubMed: 22049461]
26. Pressly ED, Pierce RA, Connal LA, Hawker CJ, Liu Y. Nanoparticle PET/CT imaging of natriuretic peptide clearance receptor in prostate cancer. *Bioconjug Chem*. 2013; 24:196–204. [PubMed: 23272904]
27. Perrier S, Takolpuckdee P. Macromolecular design via reversible addition–fragmentation chain transfer (RAFT)/xanthates (MADIX) polymerization. *J Polym Sci A Polym Chem*. 2005; 43:5347–5393.
28. Humenik M, Huang Y, Wang Y, Sprinzl M. C-terminal incorporation of bio-orthogonal azide groups into a protein and preparation of protein-oligodeoxynucleotide conjugates by Cu<sup>I</sup>-catalyzed cycloaddition. *Chembiochem*. 2007; 8:1103–1106. [PubMed: 17557370]
29. Zernecke A, Liehn EA, Gao JL, Kuziel WA, Murphy PM, Weber C. Deficiency in CCR5 but not CCR1 protects against neointima formation in atherosclerosis-prone mice: involvement of IL-10. *Blood*. 2006; 107:4240–4243. [PubMed: 16467202]

30. Westrick RJ, Winn ME, Eitzman DT. Murine models of vascular thrombosis (Eitzman series). *Arterioscler Thromb Vasc Biol.* 2007; 27:2079–2093. [PubMed: 17600224]
31. Liu Y, Ibricevic A, Cohen JA, et al. Impact of hydrogel nanoparticle size and functionalization on in vivo behavior for lung imaging and therapeutics. *Mol Pharm.* 2009; 6:1891–1902. [PubMed: 19852512]
32. Drechsler M, Duchene J, Soehnlein O. Chemokines control mobilization, recruitment, and fate of monocytes in atherosclerosis. *Arterioscler Thromb Vasc Biol.* 2015; 35:1050–1055. [PubMed: 25792446]
33. Horuk R. Promiscuous drugs as therapeutics for chemokine receptors. *Expert Rev Mol Med.* 2009; 11:e1. [PubMed: 19123963]
34. Horuk R. Chemokine receptor antagonists: overcoming developmental hurdles. *Nat Rev Drug Discov.* 2009; 8:23–33. [PubMed: 19079127]
35. Nahrendorf M, Zhang H, Hembrador S, et al. Nanoparticle PET-CT imaging of macrophages in inflammatory atherosclerosis. *Circulation.* 2008; 117:379–387. [PubMed: 18158358]
36. Moore KJ, Sheedy FJ, Fisher EA. Macrophages in atherosclerosis: a dynamic balance. *Nat Rev Immunol.* 2013; 13:709–721. [PubMed: 23995626]
37. Tarkin JM, Joshi FR, Rudd JH. PET imaging of inflammation in atherosclerosis. *Nat Rev Cardiol.* 2014; 11:443–457. [PubMed: 24913061]
38. <https://www.clinicaltrials.gov/ct2/show/NCT02498379?term=woodard&rank=1>.



**FIGURE 1.**  
Synthesis of vMIP-II-Comb ( $\alpha$ -  bromide,  vMIP-II)

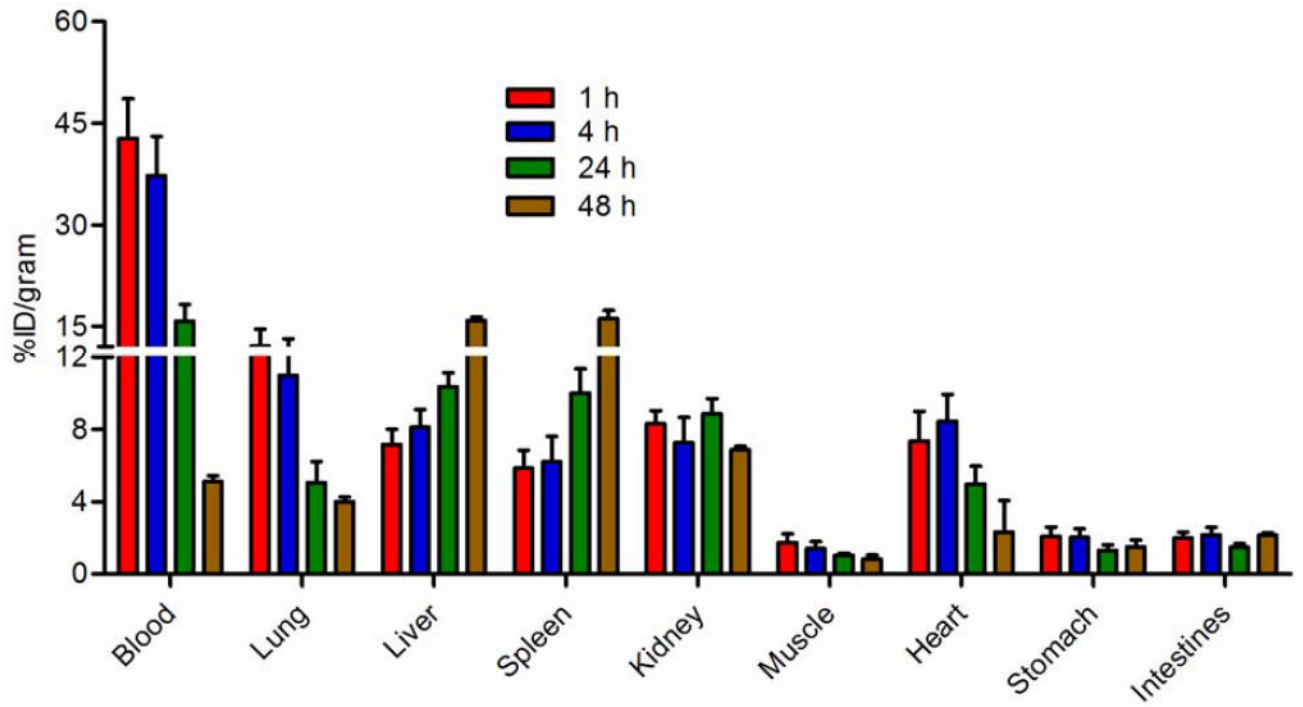


**FIGURE 2.**  
Biodistribution of  $^{64}\text{Cu}$ -vMIP-II-Comb in WT C57BL/6 mice (n=4/group).

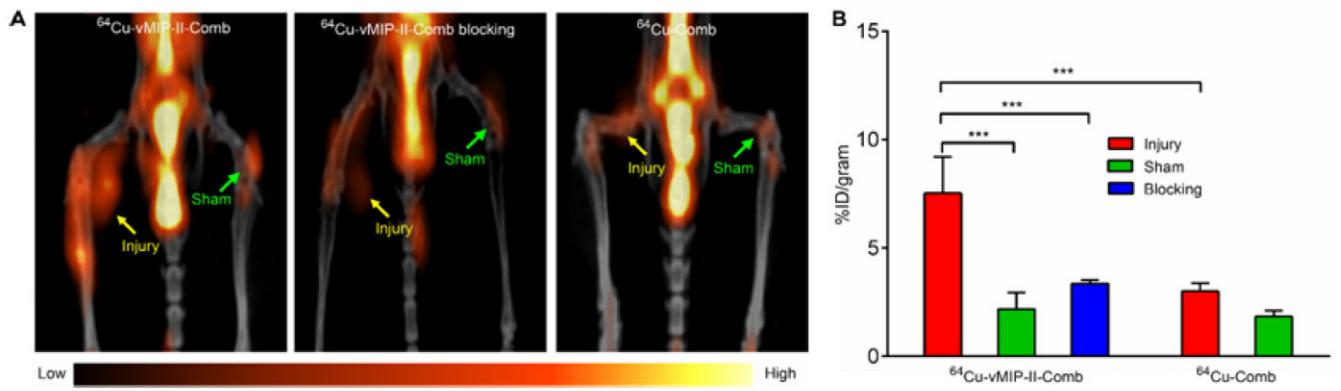


**FIGURE 3.**

(A) Representative 24 h images of  $^{64}\text{Cu-vMIP-II-Comb}$ , blocking, and  $^{64}\text{Cu-Comb}$  in injured ApoE<sup>-/-</sup> mouse. (B) Quantitative uptake analysis. \*\*\*  $P < 0.001$ ,  $n=6/\text{group}$ .



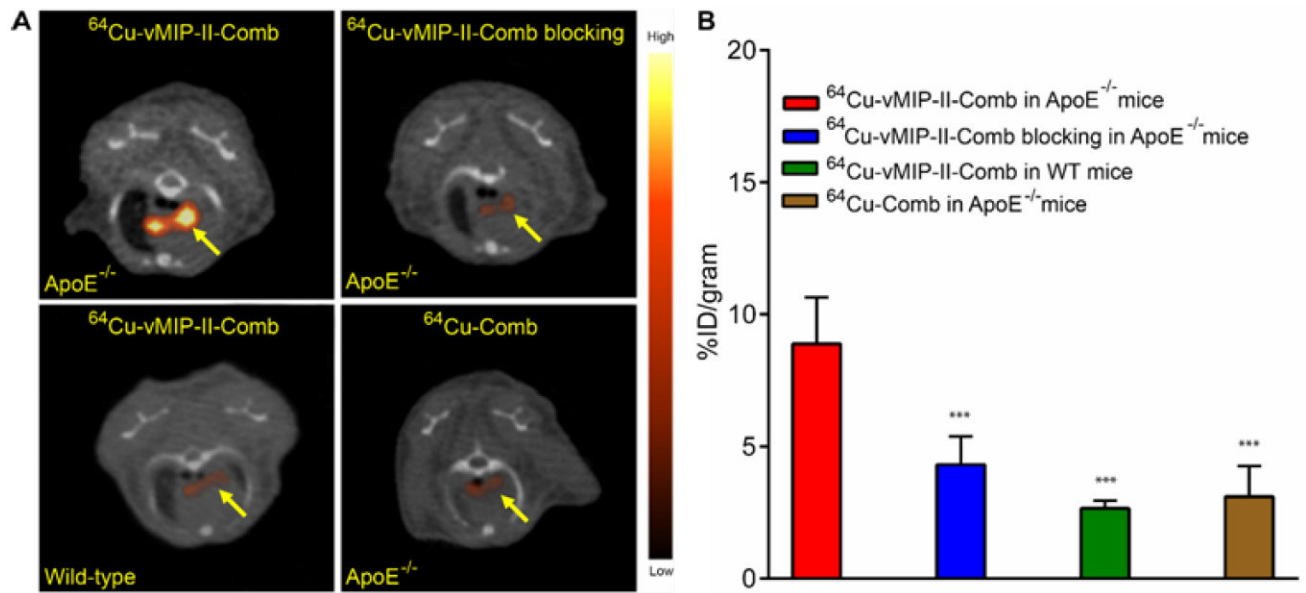


**FIGURE 4.** (A) Representative 24 h PET/CT images and (B) uptake analysis of  $^{64}\text{Cu-vMIP-II-Comb}$ , blocking, and  $^{64}\text{Cu-Comb}$  in  $\text{ApoE}^{-/-}$  mouse spontaneous atherosclerosis model. \*\*\*  $P < 0.001$ ,  $n=6/\text{group}$ .

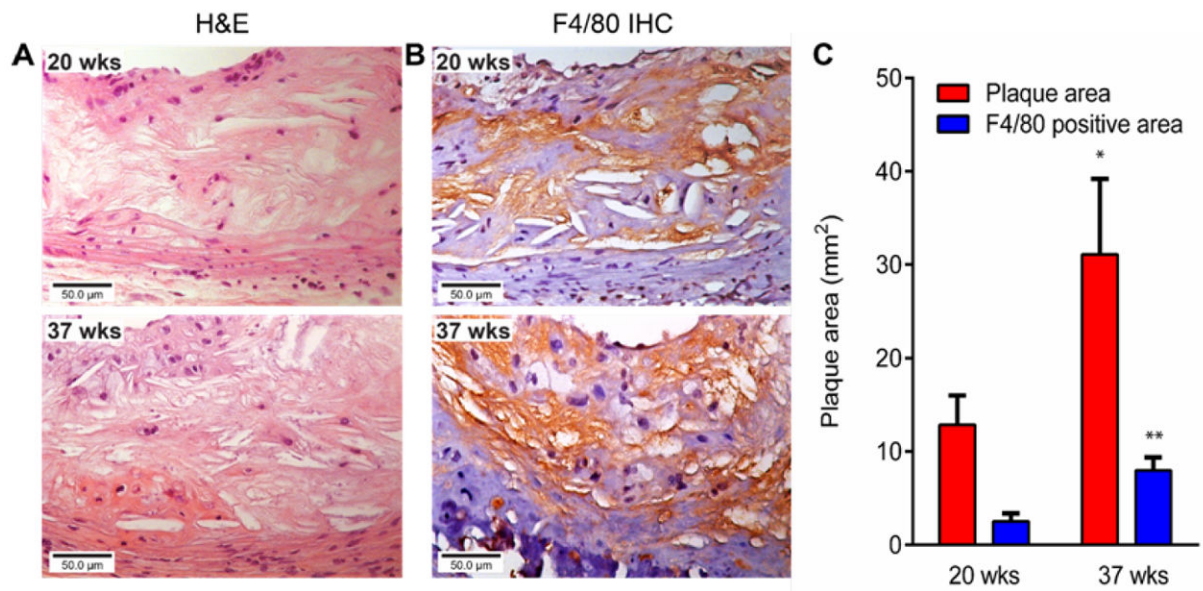


**FIGURE 5.**

Representative (A) Hematoxylin and eosin staining (40 $\times$ ) and (B) F4/80 staining (40 $\times$ ) of plaques at 20 and 37 weeks on HCD in the ApoE<sup>-/-</sup> mouse spontaneous atherosclerosis model and (C) Measurement of plaque area and F4/80 (brown) positive area at two time points (\* $P < 0.05$ , \*\*  $P < 0.005$ ,  $n=3$ /group).

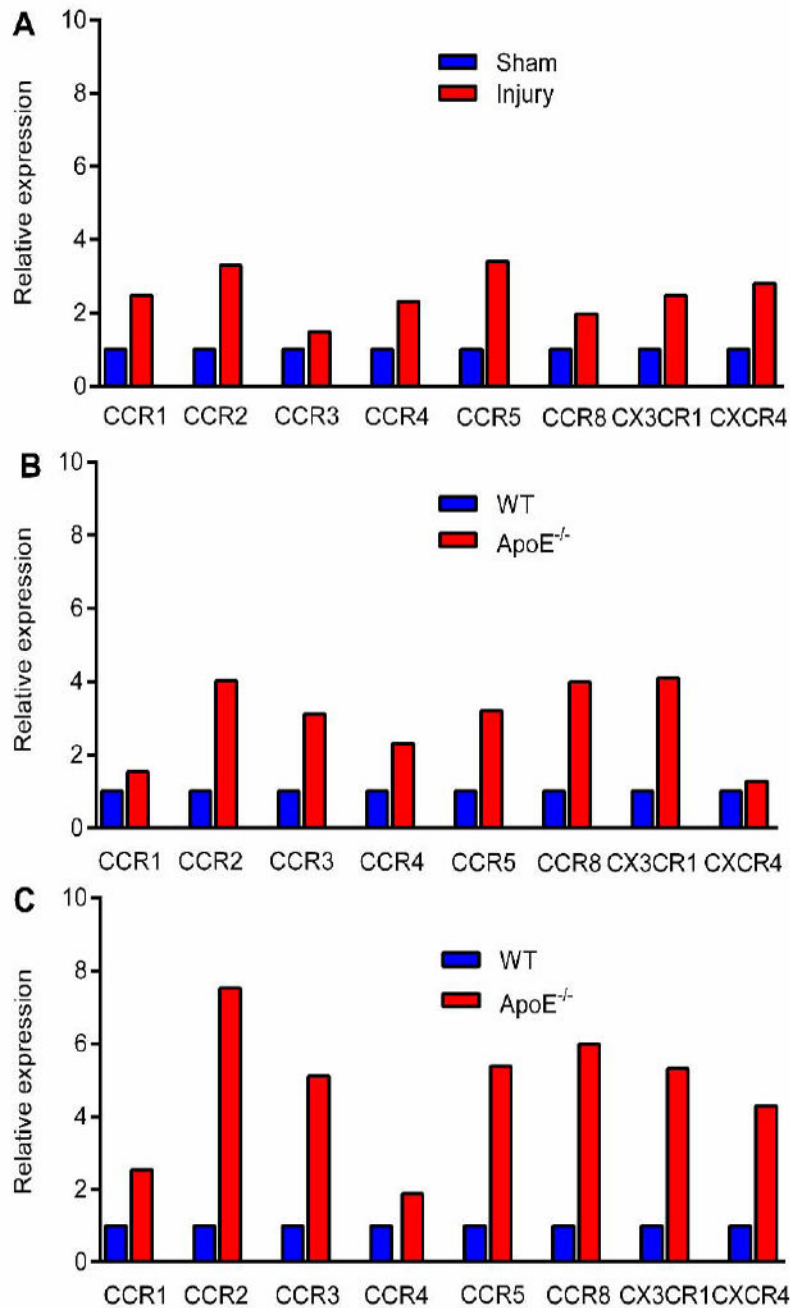


**FIGURE 6.** RT-PCR analysis of 8 chemokine receptors in (A) injured and sham-operated femoral arteries at 2 weeks post-injury in ApoE<sup>-/-</sup> mice; WT mice fed with normal chow and ApoE<sup>-/-</sup> mice fed with HCD at (B) 20 and (C) 37 weeks (n=3-5/group).